Supplementary Information (SI) for Energy & Environmental Science.

Supporting Information

Biocrust-Inspired Interface Layer with Dual Functions towards Highly Reversible Zinc Metal Anode

Huanyu Li, Yu Li, Mingquan Liu, Ziyin Yang, Yuteng Gong, Ji Qian, Ripeng Zhang, Ying Bai*, Feng Wu, Chuan Wu**

H. Li, Y. Li, M. Liu, Z. Yang, Y. Gong, J. Qian, R. Zhang, Y. Bai, F. Wu, C. Wu
Beijing Key Laboratory of Environmental Science and Engineering, School of Materials Science and Engineering, Beijing Institute of Technology, Beijing 100081, PR China.
E-mail: liyu0820@bit.edu.cn (Y. Li), membrane@bit.edu.cn (Y. Bai), chuanwu@bit.edu.cn (C. Wu)

Y. Li, M. Liu, Y. Bai, F. Wu, C. Wu
Yangtze Delta Region Academy of Beijing Institute of Technology, Jiaxing 314019, PR China.

Experimental section

Electrolyte preparation: The 2M $ZnSO_4$ electrolyte was prepared using $ZnSO_4 \cdot 7H_2O$ (General-reagent, AR>99%) and deionized water in a 100 mL volumetric flask. The DFMO/ZSO electrolytes were prepared by adding 10 mmol DFMO (MACKLIN, >98%) into 100 mL 2M $ZnSO_4$ electrolyte.

Preparation of $NaV_3O_8 \cdot 1.5H_2O$ (NVO) cathode: 0.3 g commercial V_2O_5 (Macklin) was dissolved into 10 mL 2 M NaCl (Aladdin) solution, after continuous stirring at 600 rpm for 72 h, the prepared orange red powders were washed with the deionized water and ethanol several times. Then the product was dried at 80 ℃ in the vacuum overnight. As for the Zn||NVO cell, the cathode was prepared by mixing NVO, Super P, and polyvinylidene fluoride (PVDF) at a weight ratio of 7:2:1 in N-methylpyrrolidone (NMP) solvent. Then the as-prepared slurry was coated on carbon paper or Ti foil and dried at 80 ℃ overnight under vacuum.

Materials Characterization: The scanning electron microscopy (SEM, Hitachi S8320) and transmission electron microscope (TEM, JEOL JEM-ARM200CF) were used to investigate the morphology of Zn anode and the microstructure of NVO materials. The FTIR spectra of electrolytes were obtained from Fourier transform infrared (Nicolet iS20). The Raman spectra were obtained by Horiba LabRAM HR Evolution. ^2H Nuclear magnetic resonance spectrum (NMR) were obtained by Bruker AVANCE III spectrometer. Contact angle tests were carried out by SDC 350KS. X-ray diffraction (XRD) patterns were recorded on a Rigaku Smartlab X-ray diffractometer with Cu Kα of 1.5418 Å to obtain the by-products of Zn anode. The atomic force microscopy (AFM, Bruker Dimension Fast Scan) was used to observe the morphology and roughness of the Zn anode surface. The surface composition of the Zn anode was confirmed by X-ray photoelectron spectroscopy (XPS, PHI5700) and time of flight secondary ion mass spectrometry (TOF-SIMS, PHI nano TOF II). The pH values of different electrolytes were obtained by PHSJ-6L acidometer. The operando zinc deposition microscope images were carried out with BEIYINHU U16-6550 microscope. The surface component changes of the Zn anodes during the plating/stripping/plating process were monitored by in situ Raman (Bruker RFS100/S).

Electrochemical Characterization: CR2025-type coin cells for electrochemical measurements were assembled in the air with glass fiber membrane (GF/D, Whatman) as the separator and the electrolyte amount for each coin cell was 120 µL. The two electrodes of the Zn//Zn symmetric cell were composed of metal Zn (99.99%, 100 µm), and the cathode and anode of the Zn//Cu cell were Cu foil (99.99%, 9 µm) and Zn foil, respectively. Additionally, the Zn//NVO battery was configured with NVO as the cathode (~1 mg cm^{-2}), Zn foil as the anode, and a mixed solution containing 2 M $ZnSO_4$ and DFMO as the electrolyte. The galvanostatic charge/discharge measurements were performed on a battery testing system (CT3002A, LAND, China). All Tafel, linear scan voltammetry (LSV), chronoamperograms (CA) and cyclic voltammetry (CV) were measured by an electrochemical workstation (CHI660E, Chenhua, China). Tafel plots were measured by Zn//Zn symmetric cell between –0.2 V and 0.2 V at 1 mV s^{-1}. The CA curves were measured at –0.15 V fixed overpotential. CV curves of Zn||Ti cell in 2 M $ZnSO_4$ without and with 10mM DFMO in a voltage range of –1.15 V to –0.5 V at 1 mV s^{-1}. The hydrogen evolution reaction potential was measured using LSV method with a scan rate of 1 mV s^{-1} in Na_2SO_4 and DFMO/Na_2SO_4 electrolyte.

Theoretical calculation:

Molecular dynamics (MD) simulations: The simulations for the structures of ZnSO4 electrolyte systems with and without DFMO were performed using the forcite module in Materials Studio. The information of Kennard Jones (LJ) potential parameters was taken from the condensed-phased optimized molecular potential for the atomistic simulation studies force field. One system is composed of 40 Zn^{2+}, 40 SO_4^{2-}, and 1100 H_2O molecules, while the other contains an extra 8 DFMO molecules. Moreover, a potential cutoff radius of 1.85 nm was applied within the calculation of the non-bonded interaction, and the electrostatic was represented by the atom. Each system then was equilibrated under the constant-pressure-constant-temperature (NPT) ensemble at a constant temperature of 298 K to attain an equilibrium state with zero pressure for 2000 ps. For analysis, the properties of solvated structures were received in the last 1 ns. The radial distribution functions (RDFs) were calculated using the analysis tool in Materials studio.

Finite element modeling simulations: The electrochemical secondary current distribution was calculated in the two-dimensional model. The geometric model of the experimental sample and the comparison sample is the same as the control variable, and the spatial distribution of the ion flux in the electrode region during the charging process is simulated. The two models have different physical parameters in the electrolyte region to simulate different ion migration barriers and the ionic properties of the material. The electric field in the electrolyte domain follows the constitutive relationship, the electrochemical process on the electrode surface follows the boundary conditions of the Bulter-Volmer kinetic equation, and the electrode potential follows the Nernst equation. The migration of ions follows Fick 's law and Nernst-Einstein relationship. The left and right boundaries are set as periodic conditions, and the upper boundary is an open boundary.

Density functional theory calculations: To analyze the binding energies, the density functional theory (DFT) calculations were performed using the CASTEP module. The electron exchange-correlation function was treated using a generalized gradient approximation (GGA) in the form proposed by Perdew, Burke, and Ernzerhof (PBE). The energy cutoff of the plane waves was set to 480 eV. All presented geometry optimizations are obtained until the maximum displacement below 0.005 Å, energy tolerance below 1×10^{-5} Ha, and the maximum forces lower than 0.01 eV $Å^{-1}$. A large supercell with the lattice constants larger than 12 Å along the x- and y-directions and vacuum region of about 15 Å along the z-direction was adopted. The first Brillouin zone was sampled with 2 × 2 × 1 and 3 × 3 × 1 Gamma-centered *k*-point grids for geometric optimization and electronic calculations, respectively.

The adsorption energy (E) between was defined by the following formula:

$$\mathrm{E} = E_{total} - E_{slab} - E_{Zn}$$

Where E is the total energies of molecule adsorbed with Zn. With this definition, a more negative adsorption energy indicates a more energetically favorable binding interaction of the Zn with materials. The blue and yellow regions correspond to electron accumulation and depletion, respectively.

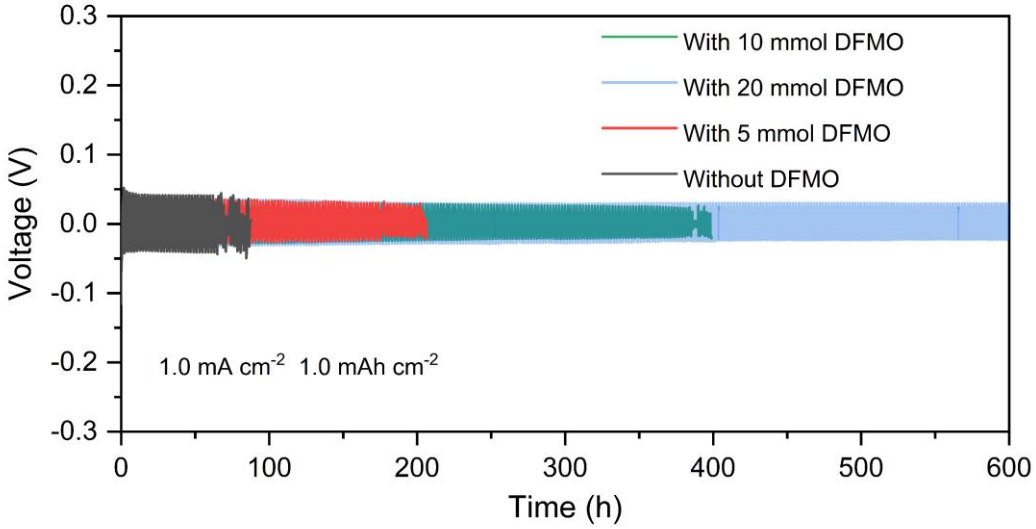

Figure S1. Cycling performance of Zn||Zn symmetrical cells in different electrolyte at 1.0 mA cm^{-2} and 1.0 mAh cm^{-2}.

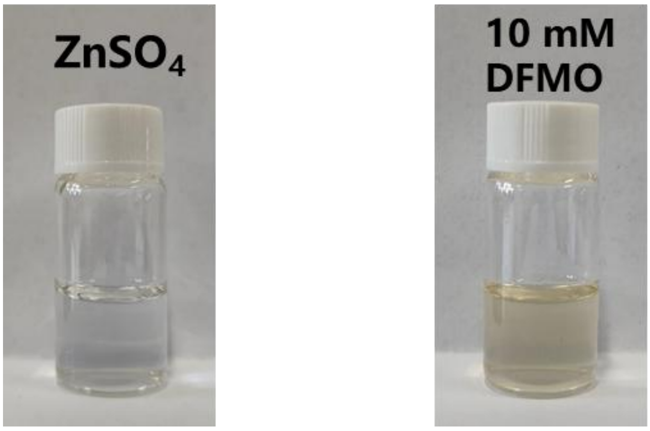

Figure S2. The digital photos for physical state of ZSO and ZSO/DFMO electrolytes.

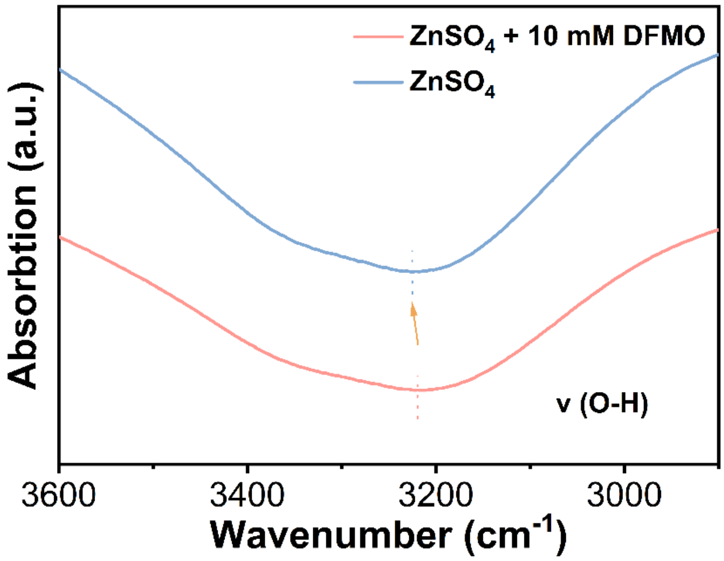

Figure S3. FTIR spectra of the electrolytes with/without DFMO.

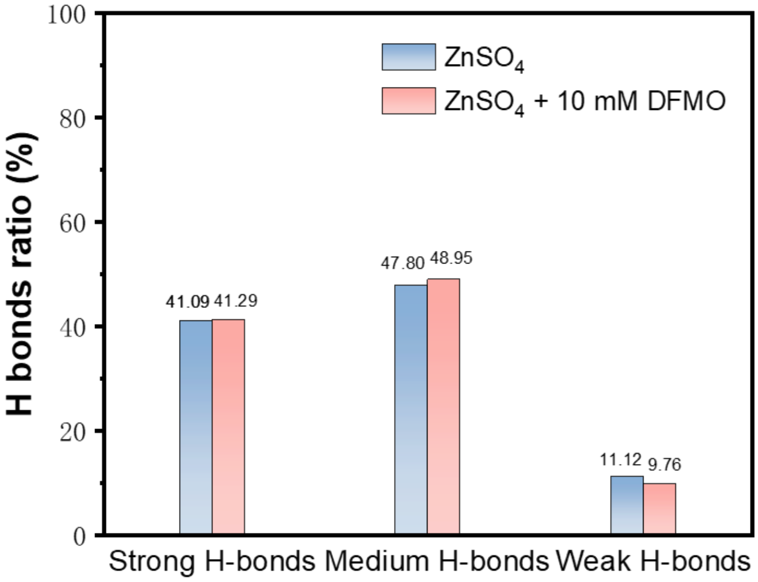

Figure S4. Measured proportions of strong, mediate, and weak H-bond in pure ZSO and ZSO/DFMO electrolytes.

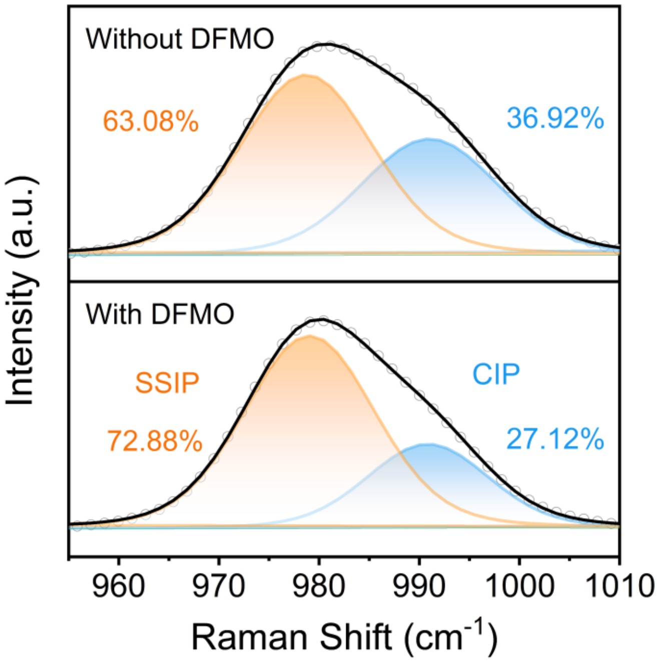

Figure S5. Fitted Raman spectra of the electrolytes with/without DFMO in the region of SO_4^{2-} band.

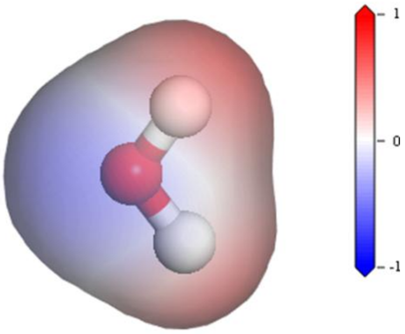

Figure S6. Electrostatic potential mapping of H_2O molecule

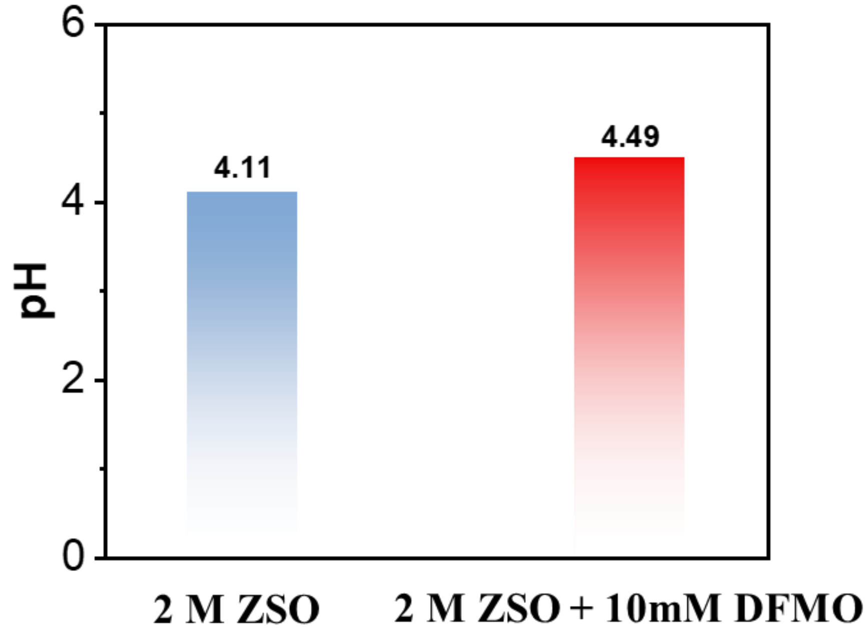

Figure S7. The pH of ZSO and ZSO/DFMO electrolytes.

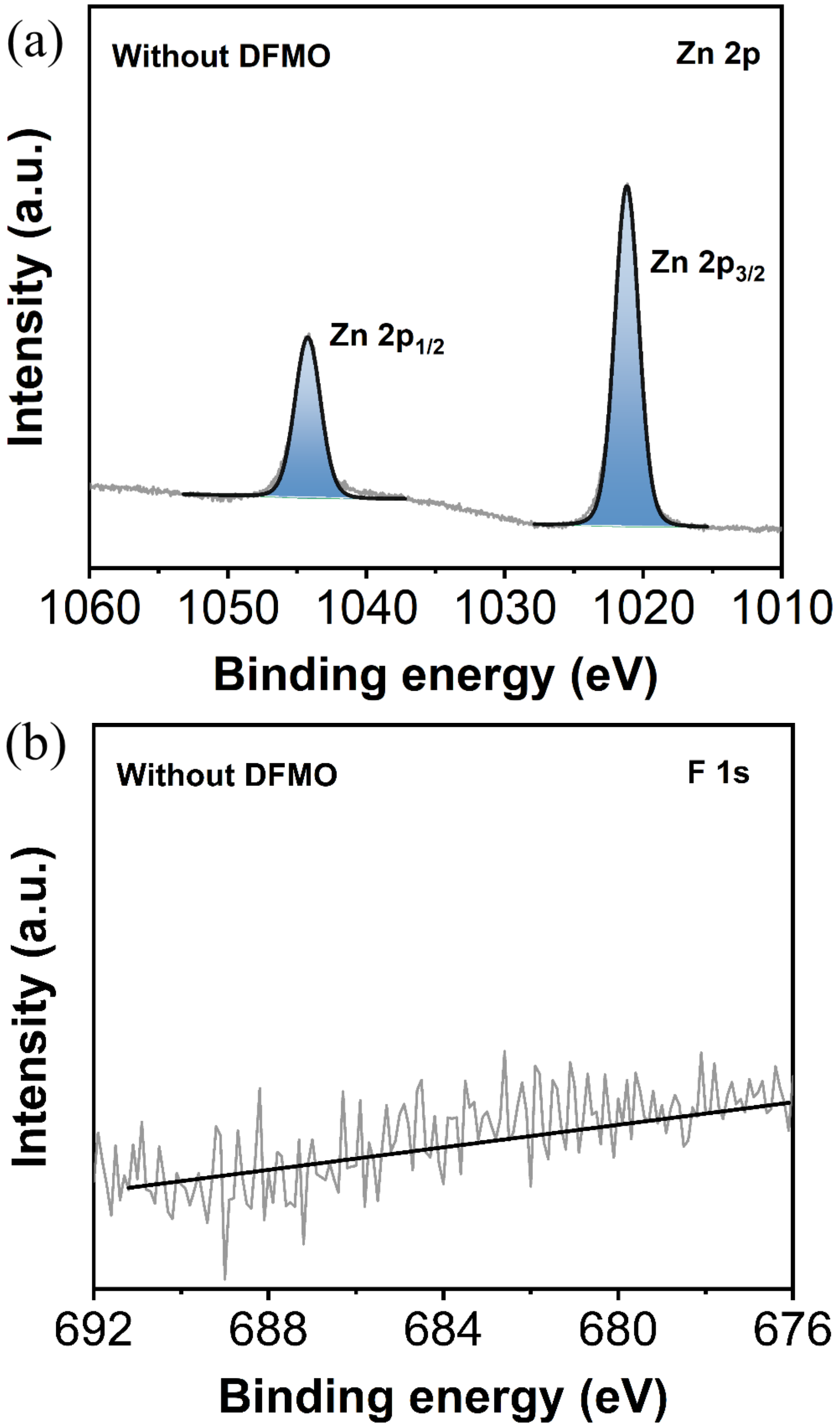

Figure S8. XPS spectra of Zn anode cycling in ZSO electrolyte (a) Zn 2p, (b) F 1s.

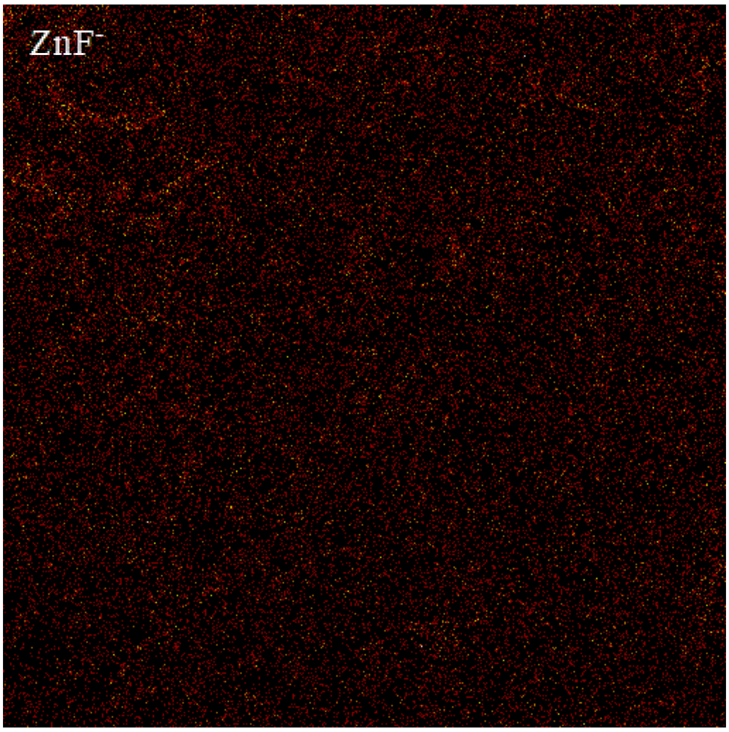

Figure S9. TOF-SIMS elemental mapping of the Zn anode after cycling in ZSO/DFMO electrolyte.

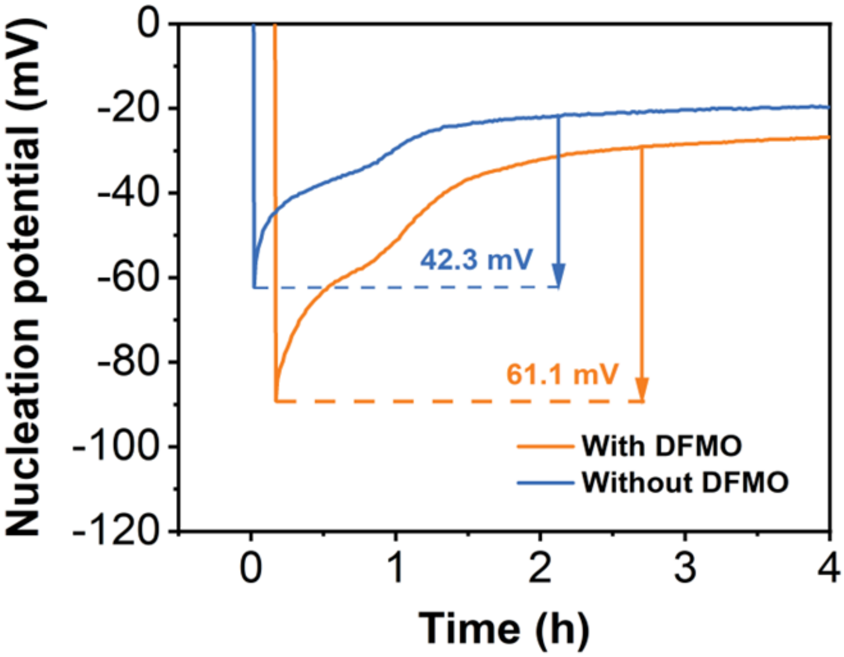

Figure S10. The initial Zn nucleation overpotentials using Zn||Ti half cells at 1 mA cm^{-2} in different electrolytes.

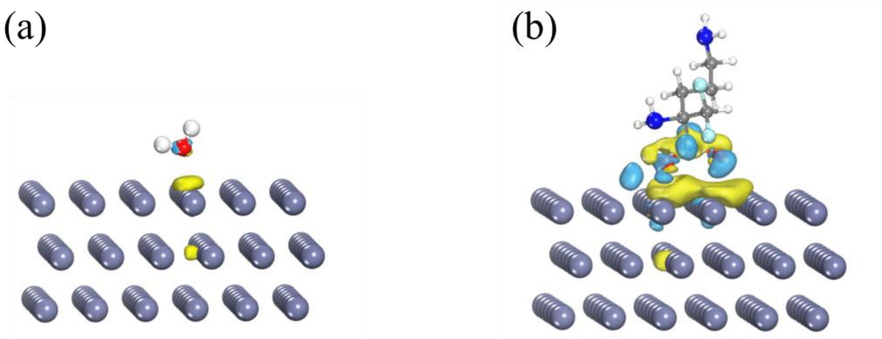

Figure S11. The charge density of (a) H_2O and (b) DFMO molecule on Zn (002) surface.

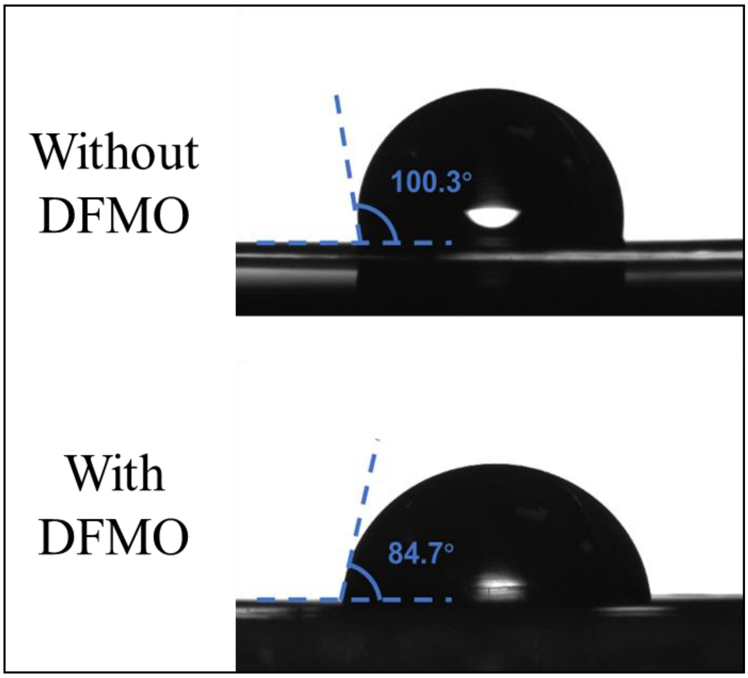

Figure S12. Contact angle test with different electrolytes.

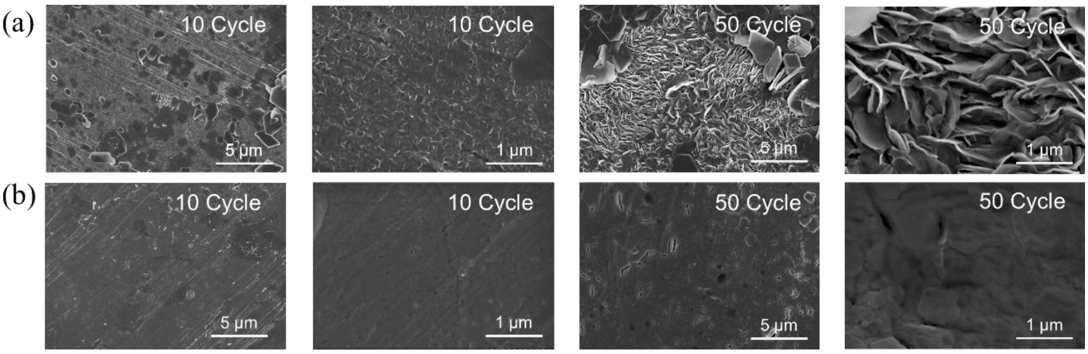

Figure S13. SEM images of the Zn anodes after cycling in (a)ZSO and (b)DFMO/ZSO electrolyte.

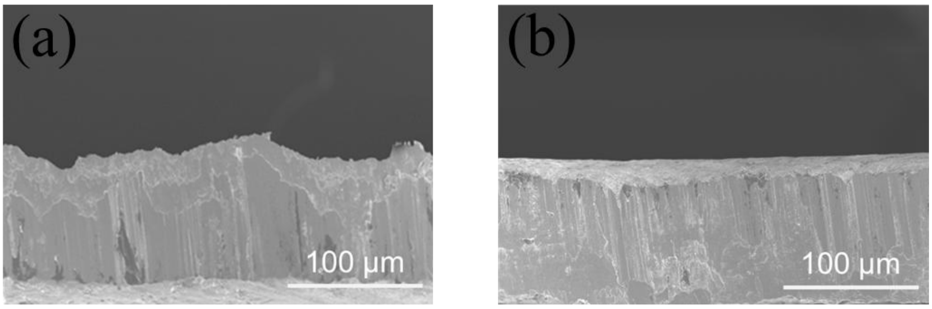

Figure S14. Cross-sectional SEM images of the Zn anode after cycling in (a)ZSO and (b)DFMO/ZSO electrolytes.

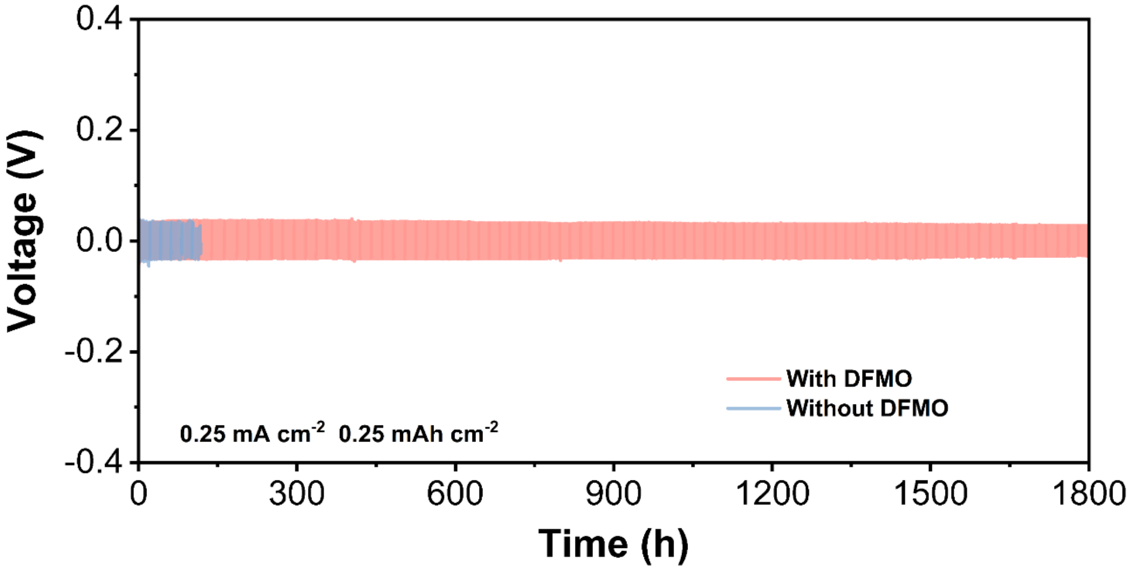

Figure S15. Galvanostatic cycling performance of Zn||Zn symmetrical cells in ZSO or ZSO/DFMO at 0.25 mA cm^{-2} and 0.25 mAh cm^{-2}.

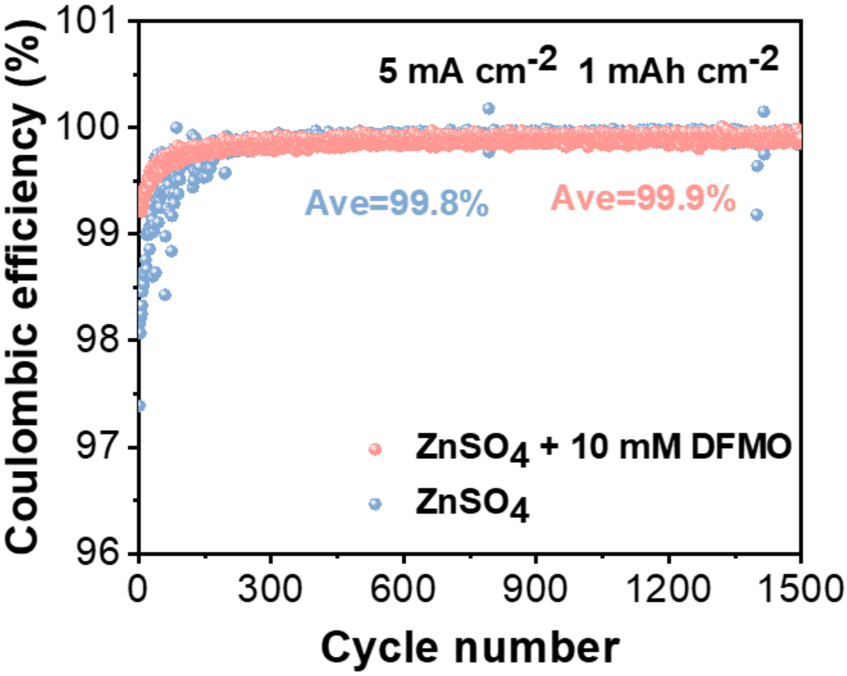

Figure S16. The CE of the Zn || Cu asymmetric cells at 5.0 mA cm^{-2} with 1.0 mAh cm^{-2}.

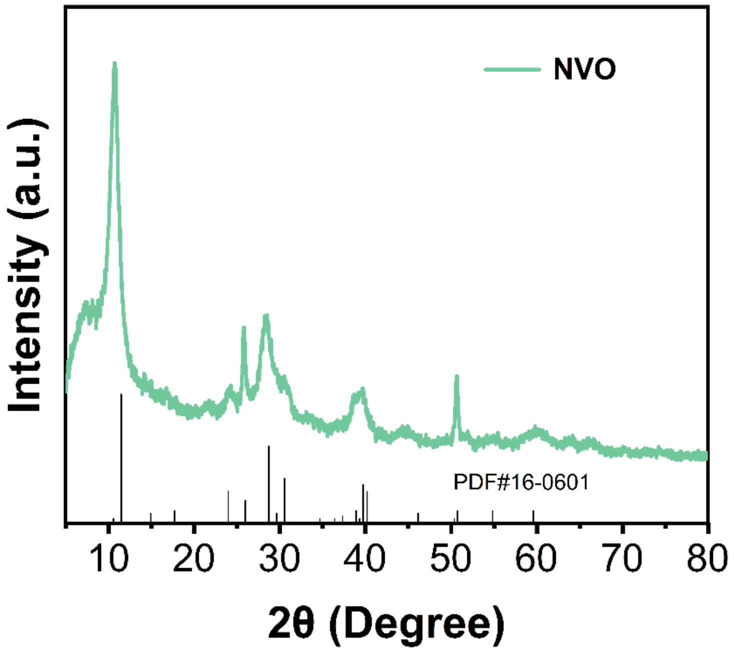

Figure S17. XRD pattern of the NVO.

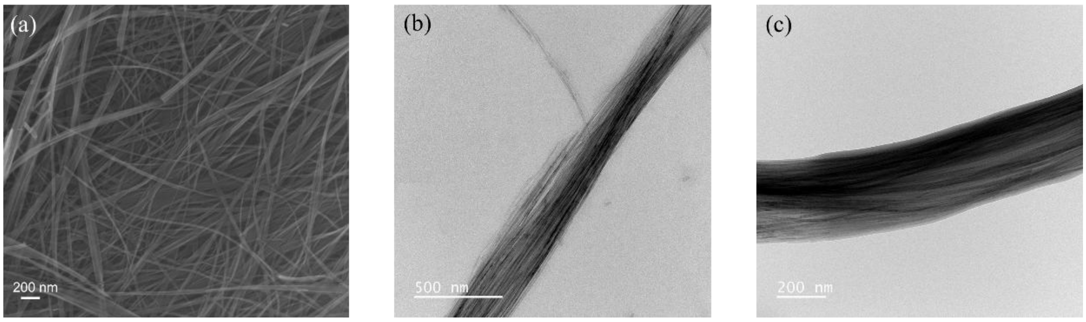

Figure S18. (a) SEM images and (b, c) TEM images of the NVO.

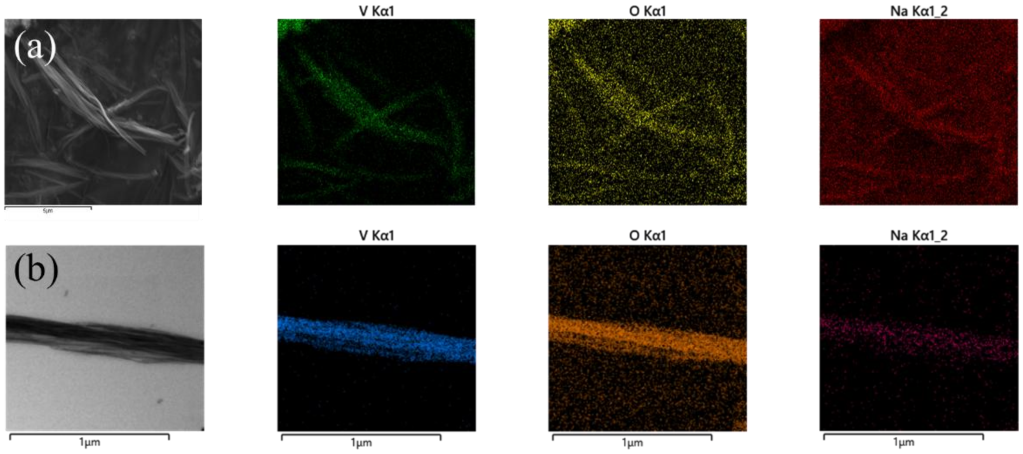

Figure S19. Elemental distribution of the NVO from (a)SEM and (b)TEM images.

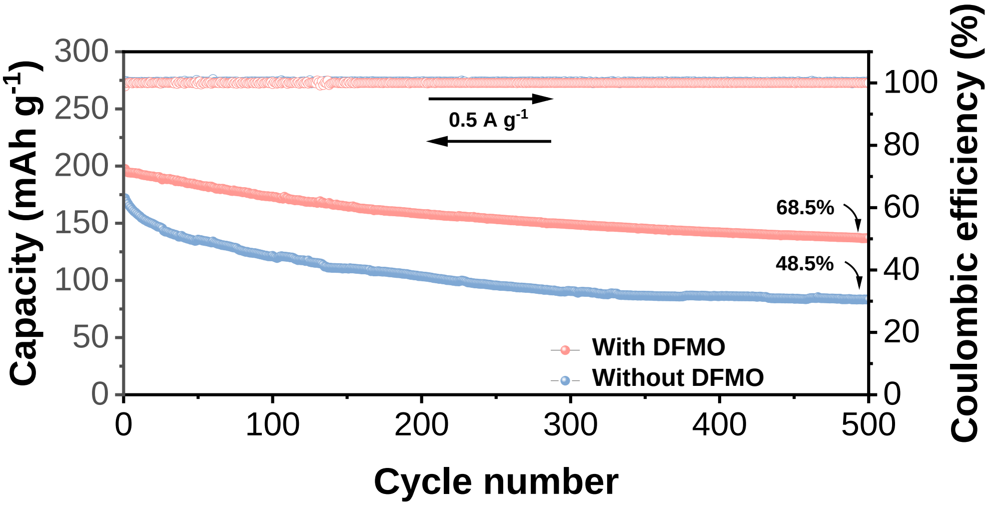

Figure S20. Cycling performance of Zn||NVO cells at 0.5 A g^{-1}.

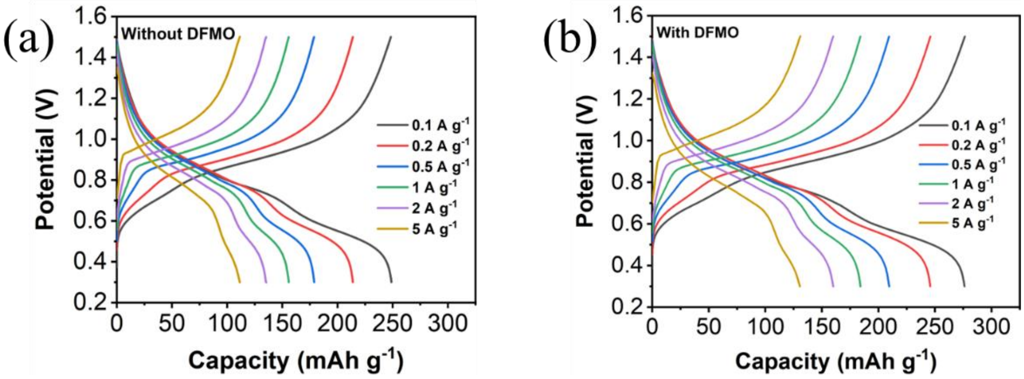

Figure S21. The charge/discharge profiles at different current density of the Zn||NVO full cells in the (a) ZSO (b) ZSO/DFMO electrolytes.

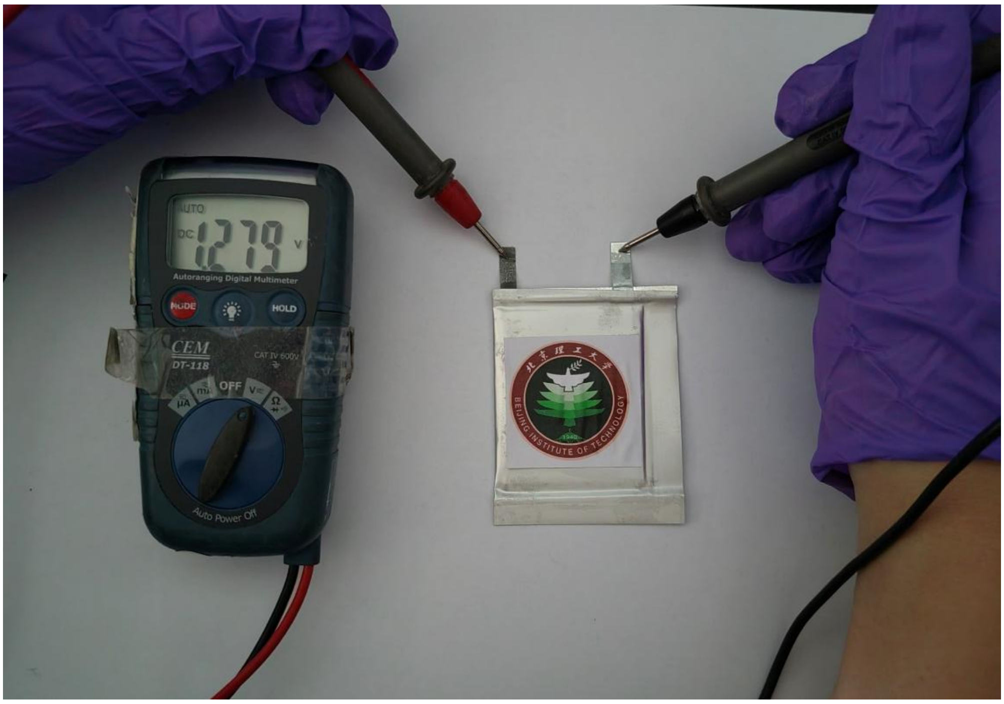

Figure S22. The digital photo for Zn||NVO pouch cell.

Table S1. The FTIR spectral data of the electrolytes with/without DFMO.

Electrolyte	v (O-H)	v (SO_4^{2-})
Without DFMO	3225.11 cm^{-1}	1079.42 cm^{-1}
With DFMO	3219.50 cm^{-1}	1077.70 cm^{-1}

Table S2. The Raman spectral data of the electrolytes with/without DFMO.

Electrolyte	Strong H-bond	Medium H-bond	Weak H-bond
Without DFMO	3247.80 cm^{-1} (41.09%)	3436.08 cm^{-1} (47.80%)	3562.01 cm^{-1} (11.11%)
With DFMO	3269.96 cm^{-1} (41.29%)	3428.21 cm^{-1} (48.95%)	3551.03 cm^{-1} (9.76%)

Table S3. The XPS spectral data of Zn anode cycling in different electrolytes.

Electrolyte	Zn 2p		F 1s
Without DFMO	Zn $2p_{1/2}$ (1044.5 eV) —	Zn $2p_{3/2}$ (1021.4 eV) —	—
With DFMO	Zn $2p_{1/2}$ (1044.5 eV) ZnF_2 (1046.1 eV)	Zn $2p_{3/2}$ (1021.4 eV) ZnF_2 (1023.0 eV)	ZnF_2 (685.2 eV)

Table S4. The comparison of the electrochemical performance of the Zn anodes in the DFMO/ZSO electrolyte with the reported works

Additive	Current density (mA cm^{-2})	Capacity (mAh cm^{-2})	Concentration (mM L^{-1})	Lifespan (h)	Ref.
trehalose	5	1	100	1600	[1]
xylitol	5	1	100	1000	[2]
sodium anthraquinone-2-sulfonate	5	1	1	1100	[3]

tetraethyl orthosilicate	5	1	20	1200	[4]
tetraethyl ammonium chloride	5	1	50	1600	[5]
threonine	5	1	10	700	[6]
zwitterionic ionic liquid	5	5	100	500	[7]
tetraphenylporphyrin tetrasulfonic acid	5	5	6	800	[8]
sodium 3,3’-dithiodipropane sulfonate	5	5	10	870	[9]
monosodium glutamate	5	5	100	1700	[10]
trehalose	5.25	5.25	5	150	[11]
succinimide	5	5	660	800	[12]
α-CD	5	5	10	200	[13]
This work	5	1	10	1954	

Reference

[1] H. Liu, Z. Xin, B. Cao, Z. Xu, B. Xu, Q. Zhu, J.-L. Yang, B. Zhang, H. J. Fan, *Adv. Funct. Mater.* **2024**, *34*, 2309840.

[2] H. Wang, W. Ye, B. Yin, K. Wang, M. S. Riaz, B.-B. Xie, Y. Zhong, Y. Hu, *Angew. Chem. Int. Ed.* **2023**, *62*, e202218872.

[3] R. Sun, D. Han, C. Cui, Z. Han, X. Guo, B. Zhang, Y. Guo, Y. Liu, Z. Weng, Q.-H. Yang, *Angew. Chem. Int. Ed.* **2023**, *62*, e202303557.

[4] N. Hu, W. Lv, H. Tang, H. Qin, Y. Zhou, L. Yi, D. Huang, Z. Wu, J. Liu, Z. Chen, J. Xu, H. He, *J. Mater. Chem. A* **2023**, *11*, 14921.

[5] T. Fang, Q. Liu, A. Hu, J. Meng, Y. Fu, Z. Shi, *J. Power Sources* **2023**, *581*, 233521.

[6] Z. Miao, Q. Liu, W. Wei, X. Zhao, M. Du, H. Li, F. Zhang, M. Hao, Z. Cui, Y. Sang, X. Wang, H. Liu, S. Wang, *Nano Energy* **2022**, *97*, 107145.

[7] Y. Lv, M. Zhao, Y. Du, Y. Kang, Y. Xiao, S. Chen, *Energy Environ. Sci.* **2022**, *15*, 4748.

[8] X. Zhao, Y. Wang, C. Huang, Y. Gao, M. Huang, Y. Ding, X. Wang, Z. Si, D. Zhou, F. Kang, *Angew. Chem. Int. Ed.* **2023**, *62*, e202312193.

[9] Y. Lin, Z. Mai, H. Liang, Y. Li, G. Yang, C. Wang, *Energy Environ. Sci.* **2023**, *16*, 687.

[10] Y. Zhong, Z. Cheng, H. Zhang, J. Li, D. Liu, Y. Liao, J. Meng, Y. Shen, Y. Huang, *Nano Energy* **2022**, *98*, 107220.

[11] H. Li, Y. Ren, Y. Zhu, J. Tian, X. Sun, C. Sheng, P. He, S. Guo, H. Zhou, *Angew. Chem. Int. Ed.* **2023**, *62*, e202310143.

[12] H. Wang, H. Du, R. Zhao, Z. Zhu, L. Qie, J. Fu, Y. Huang, *Adv. Funct. Mater.* **2023**, *33*, 2213803.

[13] K. Zhao, G. Fan, J. Liu, F. Liu, J. Li, X. Zhou, Y. Ni, M. Yu, Y.-M. Zhang, H. Su, Q. Liu, F. Cheng, *J. Am. Chem. Soc.* **2022**, *144*, 11129.